

## AN ENIGMATIC POPULATION OF LUMINOUS GLOBULAR CLUSTERS IN A GALAXY LACKING DARK MATTER

PIETER VAN DOKKUM<sup>1</sup>, YOTAM COHEN<sup>1</sup>, SHANY DANIELI<sup>1</sup>, J. M. DIEDERIK KRUIJSSEN<sup>2</sup>, AARON J. ROMANOWSKY<sup>3,4</sup>, ALLISON MERRITT<sup>5</sup>, ROBERTO ABRAHAM<sup>6</sup>, JEAN BRODIE<sup>3</sup>, CHARLIE CONROY<sup>7</sup>, DEBORAH LOKHORST<sup>6</sup>, LAMIYA MOWLA<sup>1</sup>, EWAN O’SULLIVAN<sup>7</sup>, JIELAI ZHANG<sup>6</sup>

*Accepted for publication in ApJ Letters*

### ABSTRACT

We recently found an ultra diffuse galaxy (UDG) with a half-light radius of  $R_e = 2.2$  kpc and little or no dark matter. The total mass of NGC1052–DF2 was measured from the radial velocities of bright compact objects that are associated with the galaxy. Here we analyze these objects using a combination of *HST* imaging and Keck spectroscopy. Their average size is  $\langle r_h \rangle = 6.2 \pm 0.5$  pc and their average ellipticity is  $\langle \epsilon \rangle = 0.18 \pm 0.02$ . From a stacked Keck spectrum we derive an age of  $\gtrsim 9$  Gyr and a metallicity of  $[\text{Fe}/\text{H}] = -1.35 \pm 0.12$ . Their properties are similar to  $\omega$  Centauri, the brightest and largest globular cluster in the Milky Way, and our results demonstrate that the luminosity function of metal-poor globular clusters is not universal. The fraction of the total stellar mass that is in the globular cluster system is similar to that in other UDGs, and consistent with “failed galaxy” scenarios where star formation terminated shortly after the clusters were formed. However, the galaxy is a factor of  $\sim 1000$  removed from the relation between globular cluster mass and total galaxy mass that has been found for other galaxies, including other UDGs. We infer that a dark matter halo is not a prerequisite for the formation of metal-poor globular cluster-like objects in high redshift galaxies.

*Keywords:* galaxies: evolution — galaxies: structure

### 1. INTRODUCTION

We recently identified a galaxy with little or no dark matter (van Dokkum et al. 2018, hereafter vD18). NGC1052–DF2 has a stellar mass of  $M_{\text{stars}} \approx 2 \times 10^8 M_{\odot}$  and a 90% confidence upper limit on its dark matter halo mass of  $M_{\text{halo}} < 1.5 \times 10^8 M_{\odot}$ , placing it a factor of  $\gtrsim 400$  off of the canonical stellar mass – halo mass relation (Moster et al. 2013; Behroozi et al. 2013). NGC1052–DF2 is a featureless, spheroidal “ultra diffuse” galaxy (UDG; van Dokkum et al. 2015), with an effective radius of  $R_e = 2.2$  kpc and a central surface brightness  $\mu(V_{606}, 0) = 24.4$  mag arcsec<sup>−2</sup>. It has a radial velocity of 1803 km s<sup>−1</sup>. Its SBF-determined distance is  $19.0 \pm 1.7$  Mpc (vD18), consistent with that of the NGC 1052 group at  $D \approx 20$  Mpc (Blakeslee et al. 2010).

The kinematics of NGC1052–DF2 were measured from the radial velocities of 10 compact objects that are associated with the galaxy. These objects drew our attention to the galaxy in the first place: it is a large, low surface brightness blob in our Dragonfly Telephoto Array imag-

ing (Abraham & van Dokkum 2014; Merritt et al. 2016) but a collection of point-like sources in the Sloan Digital Sky Survey.

Finding globular clusters (GCs) in a UDG is in itself not unusual (Beasley et al. 2016; Peng & Lim 2016; van Dokkum et al. 2016, 2017; Amorisco, Monachesi, & White 2018). In fact, Coma UDGs have on average  $\sim 7$  times more GCs than other galaxies of the same luminosity (van Dokkum et al. 2017), with large galaxy-to-galaxy scatter (Amorisco et al. 2018). However, what is unusual, or at least unexpected, is the remarkable luminosity of the clusters. The luminosity function of the GC populations of Coma UDGs is consistent with that seen in other galaxies, peaking at an absolute magnitude  $M_V \sim -7.5$  (Peng & Lim 2016; van Dokkum et al. 2017; Amorisco et al. 2018). The ten clusters that were analyzed in vD18 are all significantly brighter than this, raising the question whether the GC luminosity function is systematically offset from that in other galaxies.

Here we focus on the properties of the compact objects in NGC1052–DF2, using imaging from the *Hubble Space Telescope* (*HST*) and spectroscopy obtained with the W. M. Keck Observatory. We show that the GC system of NGC1052–DF2 is unprecedented, both in terms of the average properties of the clusters and in its offset from the canonical scaling relation between GC system mass and total galaxy mass.

### 2. IDENTIFICATION

#### 2.1. Spectroscopically-Identified Clusters

We obtained spectra of compact objects in the NGC1052–DF2 region with the Keck telescopes, using the Deep Imaging Multi-Object Spectrograph on Keck II, the red arm of the Low-Resolution Imaging Spectrometer (LRIS; Oke et al. 1995), and the blue arm of

<sup>1</sup> Astronomy Department, Yale University, 52 Hillhouse Ave, New Haven, CT 06511, USA

<sup>2</sup> Astronomisches Rechen-Institut, Zentrum für Astronomie der Universität Heidelberg, Mönchhofstraße 12-14, D-69120 Heidelberg, Germany

<sup>3</sup> University of California Observatories, 1156 High Street, Santa Cruz, CA 95064, USA

<sup>4</sup> Department of Physics and Astronomy, San José State University, San Jose, CA 95192, USA

<sup>5</sup> Max-Planck-Institut für Astronomie, Königstuhl 17, D-69117 Heidelberg, Germany

<sup>6</sup> Department of Astronomy & Astrophysics, University of Toronto, 50 St. George Street, Toronto, ON M5S 3H4, Canada

<sup>7</sup> Harvard-Smithsonian Center for Astrophysics, 60 Garden Street, Cambridge, MA, USA

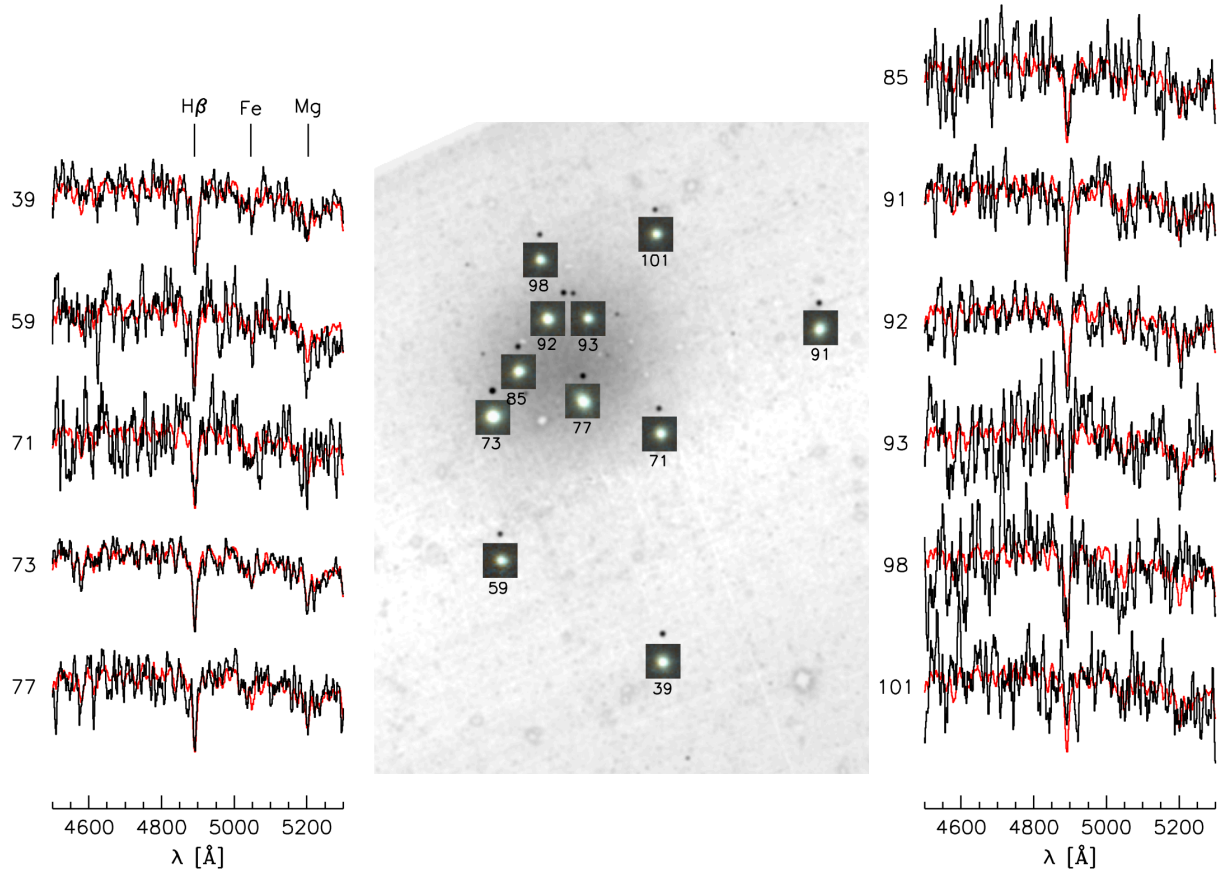


**Figure 1.** Keck/LRIS spectra (left and right) and *HST* images (center) of the 11 clusters associated with NGC1052–DF2. The color images, generated from the  $V_{606}$  and  $I_{814}$  data, span  $1'' \times 1''$ . Some of the clusters are visibly flattened. The background image was generated by masking all objects in the  $I_{814}$  *HST* frame that do not match the color and size criteria we use for selecting GCs, and then applying a slight smoothing to emphasize the compact objects. The spectra focus on the wavelength region around the redshifted  $\lambda 4861$  H $\beta$  and  $\lambda 5172$  Mg lines. The red line is a S/N-weighted average of the 11 spectra.

LRIS. The sample selection, reduction, and analysis of the high resolution DEIMOS and red LRIS data are described in detail in vD18. The blue-side LRIS data were obtained with the 300/5000 grism and  $1''0$  slits, providing a spectral resolution ranging from  $\sigma_{\text{instr}} \sim 350 \text{ km s}^{-1}$  at  $\lambda = 3800 \text{ \AA}$  to  $\sigma_{\text{instr}} \sim 150 \text{ km s}^{-1}$  at  $\lambda = 6600 \text{ \AA}$ . The reduction followed the same procedures as the red side data, and is described in vD18. The spectral resolution is too low for accurate radial velocity measurements, but the wide wavelength coverage provides constraints on the stellar populations (§ 5). Small sections of the spectra of the 11 confirmed GCs are shown in Fig. 1. Note that we analyze one more object in this paper than in vD18; this is because the S/N ratio of the red spectrum of GC-93 is too low for an accurate velocity measurement.<sup>8</sup>

## 2.2. Photometrically-Identified Clusters

To measure the luminosity function we also have to consider GCs that are fainter than the spectroscopic limits, as well as any that might not have been included in the masks. We select all candidate GCs using the  $V_{606}$  and  $I_{814}$  *HST* images (described in vD18). Photometric catalogs were created using SExtractor (Bertin

& Arnouts 1996) in dual image mode. The photometry was corrected for Galactic extinction (Schlafley & Finkbeiner 2011), and the  $V_{606} - I_{814}$  colors were corrected for the wavelength dependence of the PSF. Total magnitudes were determined from the “AUTO” fluxes, with an object-by-object correction to an infinite aperture as determined from the encircled energy curves of Bohlin (2016).

The top panel in Fig. 2 shows all objects with  $I_{814} < 26.5$  in the plane of  $V_{606} - I_{814}$  color vs.  $I_{814}$  magnitude. The 11 spectroscopically-identified clusters have a remarkably small range in color: we find  $\langle V_{606} - I_{814} \rangle = 0.36$  with an observed rms scatter of  $\sigma_{V-I} = 0.039$ . This is not a result of selection; we obtained spectra of nearly all compact objects in the vicinity of NGC1052–DF2 irrespective of their color. The bottom panel of Fig. 2 shows the relation between the SExtractor FWHM and  $I_{814}$  magnitude for all objects that have colors in the range  $\langle V_{606} - I_{814} \rangle \pm 2\sigma_{V-I}$ . We note that the results are not sensitive to the precise limits that are used here. As expected, the spectroscopically-identified GCs are small. The dashed line corresponds to  $\text{FWHM} < \langle \text{FWHM} \rangle + 2.5\sigma_{\text{FWHM}} = 4.7$  pixels.

We find that the spectroscopic completeness is 100% for  $I_{814} < 23$  objects that satisfy the color and size criteria. We find 16 candidate GCs with  $23 < I_{814} < 25.5$ ,

<sup>8</sup> Oddly the red side spectrum of GC-93 appears to be featureless in the Ca triplet region.

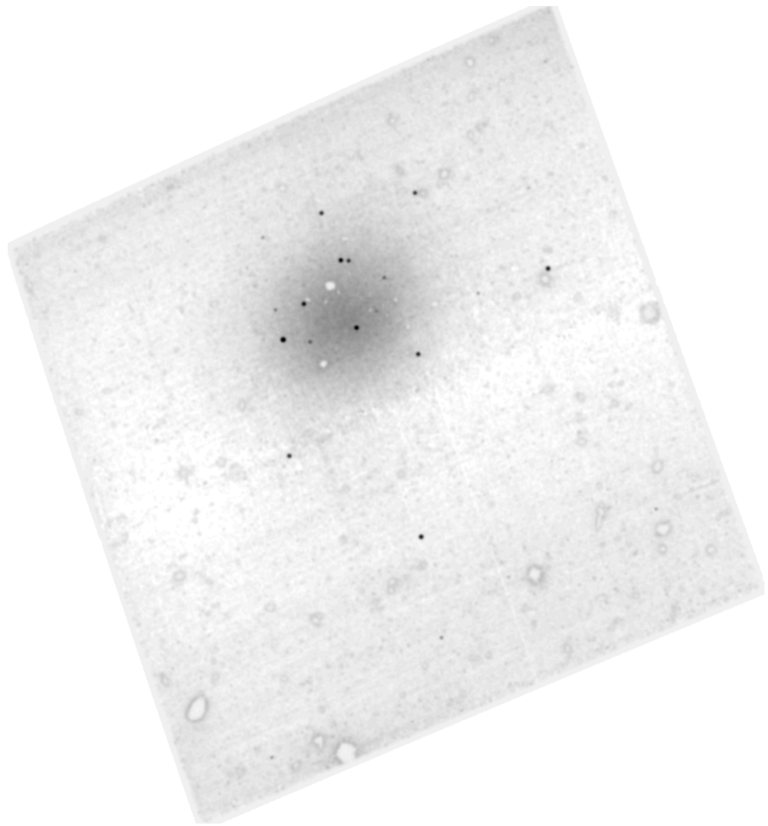
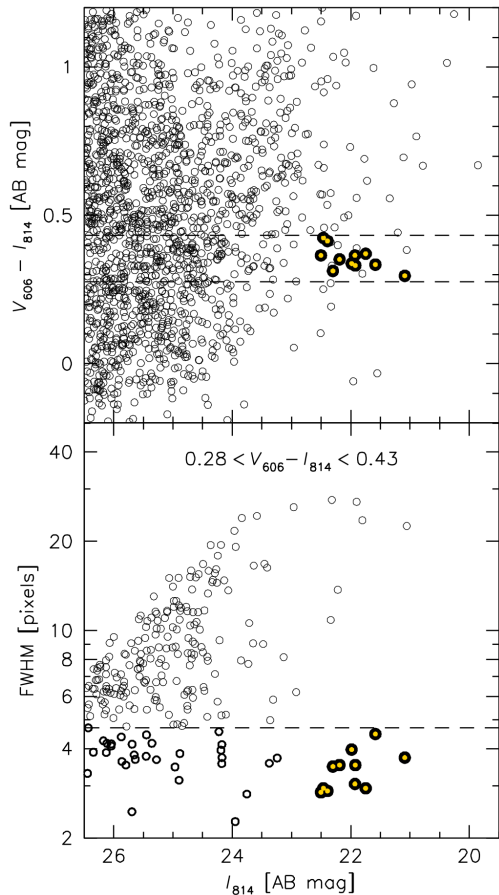


**Figure 2.** Photometric selection of globular clusters. The top panel shows the color-magnitude relation of all objects in the *HST* images of NGC1052-DF2. The 11 spectroscopically-confirmed objects are marked with yellow and black circles. Dashed lines delineate the  $\pm 2\sigma$  range of the colors of the confirmed clusters:  $0.28 < V_{606} - I_{814} < 0.43$ . The bottom panel shows the size-magnitude relation for all objects that satisfy this color criterion. Objects with  $\text{FWHM} < 4.7$  pixels are candidate GCs. The image on the right is a wider view of that shown in Fig. 1. All objects are masked, except those that match the color and size criteria.

but as we show below most are probably compact background galaxies. The grey scale panel of Fig. 2 shows the  $I_{814}$  data after masking all objects that do *not* satisfy these criteria. The masked image was smoothed with a Gaussian of  $\text{FWHM} = 0''.9$ .

### 3. LUMINOSITY FUNCTION AND SPECIFIC FREQUENCY

At bright magnitudes it is straightforward to measure the luminosity function of the GCs because the spectroscopic completeness is 100%, but at  $I_{814} > 23$  a correction needs to be made for interlopers. This is evident from the distribution of objects in the bottom panel of Fig. 2: at  $I_{814} < 23$  the GCs are well-separated from other objects, but at faint magnitudes there is a continuous distribution of sources with  $\text{FWHM} \sim 2 - 15$  pixels. This magnitude-dependent correction for unrelated objects was determined from ACS imaging obtained in the blank field CANDELS survey (Koekemoer et al. 2011). We obtained CANDELS  $V_{606}$  and  $I_{814}$  images of the AEGIS field from the 3D-HST data release (Skelton et al. 2014), and analyzed these in the exact same way as the NGC1052-DF2 data.

The results are shown in the top panels of Fig. 3. The expected contamination increases steadily with magnitude at  $I_{814} > 23$ . The top right panel shows the ob-

served magnitude distribution after subtracting the expected contamination, with the uncertainties reflecting the Poisson errors in the observed counts in each bin. There is a pronounced peak at  $I_{814} = 22.0$  with a  $1\sigma$  width of 0.4 mag, consisting of the 11 confirmed clusters.

The bottom panel of Fig. 3 shows the luminosity function. For consistency with other work we focus on  $M_{V,606}$ , determined from the total  $I_{814}$  magnitudes through  $M_{V,606} = I_{814} + (V_{606} - I_{814}) - 31.50$ . The mean absolute magnitude of the confirmed clusters is  $M_{V,606} = -9.1$ , and the brightest cluster (GC-73) has  $M_{V,606} = -10.1$ . The red curve shows the (scaled) luminosity function of Milky Way GCs, obtained from the 2010 edition of the Harris (1996) catalog<sup>9</sup> with  $M_{V,606} = M_V - 0.05$ . The peak magnitude of  $M_V \sim -7.5$  for the Milky Way is similar to that seen in other galaxies (e.g., Rejkuba 2012). The blue curve is the average luminosity function of GCs in the two UDGs Dragonfly 44 and DFX1, taken from van Dokkum et al. (2017).

The luminosity function of NGC1052-DF2 is shifted to higher luminosities than those of other galaxies, including other UDGs. The difference is a factor of  $\sim 4$ . Phrased differently, the GC luminosity function of NGC1052-DF2 is not far removed from the

<sup>9</sup> <http://physwww.mcmaster.ca/~harris/mwgc.dat>

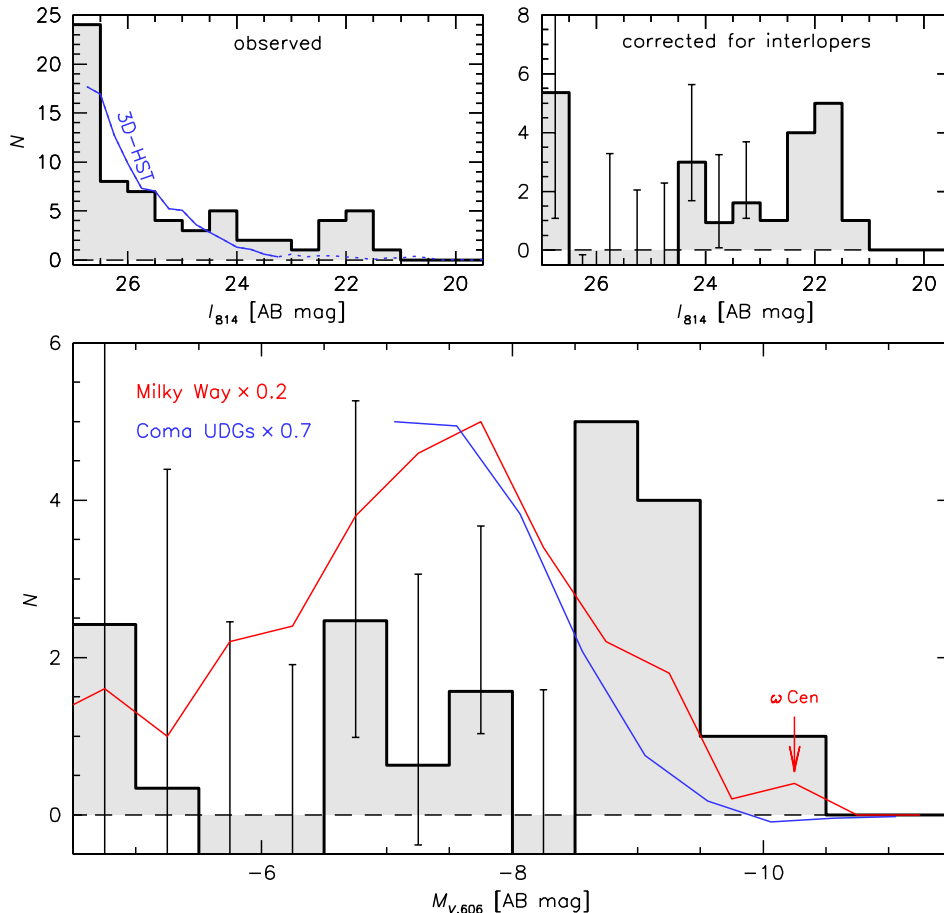


**Figure 3.** Luminosity function of the compact objects in NGC1052–DF2. *Top left:* Observed luminosity function, in apparent  $I_{814}$  magnitude. The blue line shows the magnitude distribution of objects in blank field 3D-HST/CANDELS imaging that have the same colors and sizes as the GCs. *Top right:* Observed luminosity function, after correcting each bin for the expected number of unrelated objects. *Bottom:* Luminosity function in absolute magnitude, for  $D = 20$  Mpc. The luminosity functions of GCs in the Milky Way and in Coma UDGs are shown in red and blue, respectively.

bright end of the luminosity function of the Milky Way: NGC1052–DF2 has 11 clusters brighter than  $M_{V,606} = -8.6$ , whereas the Milky Way has 20 (and only 15 with  $[\text{Fe}/\text{H}] < -1$ ). However, there is only marginal evidence for the presence of “classical” GCs with  $M_{V,606} \sim -7.5$  in NGC1052–DF2: after correcting for interlopers, the total number of GCs with  $-8.5 < M_{V,606} < -6.5$  is  $N_{\text{peak}} = 4.2^{+3.4}_{-2.1}$  (compared to  $N_{\text{peak}} = 84$  in the Milky Way).

Taking the total number of globular clusters as  $\approx 15$ , we derive a specific frequency  $S_N \equiv N_{\text{GC}} \times 10^{0.4(M_V^g + 15)} \approx 11$ , where  $M_V^g = -15.4$  is the total magnitude of the galaxy (see vD18). The 11 spectroscopically-confirmed clusters constitute 4% of the total luminosity of NGC1052–DF2 (with 1% contributed by GC-73 and 3% by the other clusters).

#### 4. STRUCTURAL PARAMETERS

We use the *HST* imaging to compare the morphologies of the NGC1052–DF2 GCs to those of Milky Way GCs. We fit King (1962) models to the individual .f1c files using the GALFIT software (Peng et al. 2002) with synthetic PSFs. This provides eight independent measurements (four in  $V_{606}$  and four in  $I_{814}$ ). Cosmic rays

and neighboring objects were masked in the fits.

The results are listed in Table 1. Circularized half-light radii  $r_h$  were determined from the measured core and tidal radii (multiplied by  $\sqrt{b/a}$ ). The listed values are the biweight averages (see Beers, Flynn, & Gebhardt 1990) of the eight individual measurements, and for each entry the listed error is the biweight scatter in the eight individual measurements. We verified that very similar values are obtained if a Sersic (1968) profile is fitted to the objects instead of a King profile. As a test of our ability to measure the sizes of these small objects we also included four stars of similar brightness to the GCs in the fits. All four stars have  $r_h < 0''.018$ , whereas the GCs have sizes in the range  $0''.043 \leq r_h \leq 0''.089$ .

The sizes and ellipticities are compared to those of Milky Way GCs in Fig. 4, again making use of the 2010 version of the Harris (1996) compilation. The (biweight) mean size of the 11 objects is  $\langle r_h \rangle = 6.2 \pm 0.5$  pc, a factor of 2.2 larger than the mean size of Milky Way GCs in the same luminosity range. The mean ellipticity is  $\langle \epsilon \rangle = 0.18 \pm 0.02$ , a factor of 2.6 larger than Milky Way GCs.

#### 5. STELLAR POPULATIONS

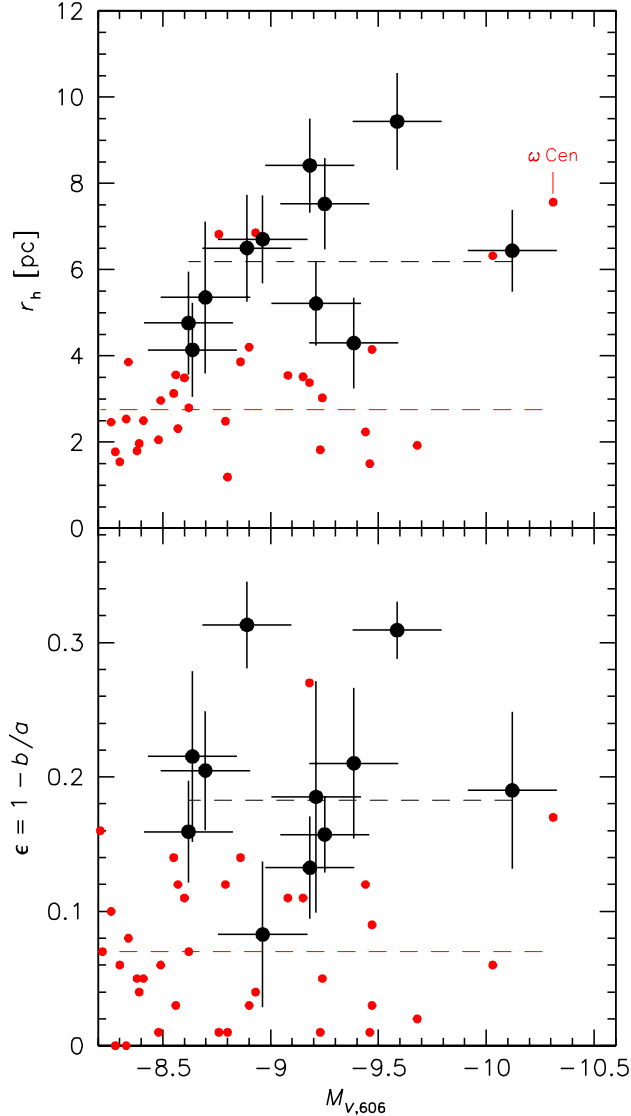


**Figure 4.** Morphological parameters of the GCs. The top panel shows the circularized half-light radii versus the absolute magnitude, for NGC1052–DF2 (black points with error bars) and the Milky Way (red). Errors in  $M_{V,606}$  and  $r_h$  include a 10% uncertainty in the distance (see vD18). The bottom panel shows the ellipticity. Means are indicated with dashed lines.

**Table 1**  
Properties Of Globular Clusters

Id	RA	DEC	$M_{V,606}$	$r_h^a$	$\epsilon$
39	2 <sup>h</sup> 41 <sup>m</sup> 45.07 <sup>s</sup>	–8°25′24″.9	–9.3	7.5 ± 0.7	0.16 ± 0.03
59	2 <sup>h</sup> 41 <sup>m</sup> 48.08 <sup>s</sup>	–8°24′57″.5	–8.9	6.5 ± 1.0	0.31 ± 0.03
71	2 <sup>h</sup> 41 <sup>m</sup> 45.13 <sup>s</sup>	–8°24′23″.0	–9.0	6.7 ± 0.8	0.08 ± 0.05
73	2 <sup>h</sup> 41 <sup>m</sup> 48.22 <sup>s</sup>	–8°24′18″.1	–10.1	6.4 ± 0.7	0.19 ± 0.06
77	2 <sup>h</sup> 41 <sup>m</sup> 46.54 <sup>s</sup>	–8°24′14″.0	–9.6	9.4 ± 0.6	0.31 ± 0.02
85	2 <sup>h</sup> 41 <sup>m</sup> 47.75 <sup>s</sup>	–8°24′05″.9	–9.2	5.2 ± 0.8	0.19 ± 0.09
91	2 <sup>h</sup> 41 <sup>m</sup> 42.17 <sup>s</sup>	–8°23′54″.0	–9.2	8.4 ± 0.7	0.13 ± 0.04
93	2 <sup>h</sup> 41 <sup>m</sup> 46.72 <sup>s</sup>	–8°23′51″.3	–8.6	4.1 ± 1.0	0.22 ± 0.06
92	2 <sup>h</sup> 41 <sup>m</sup> 46.90 <sup>s</sup>	–8°23′51″.1	–9.4	4.3 ± 1.0	0.21 ± 0.06
98	2 <sup>h</sup> 41 <sup>m</sup> 47.34 <sup>s</sup>	–8°23′35″.2	–8.7	5.4 ± 1.7	0.20 ± 0.04
101	2 <sup>h</sup> 41 <sup>m</sup> 45.21 <sup>s</sup>	–8°23′28″.3	–8.6	4.8 ± 1.1	0.16 ± 0.04

<sup>a</sup> Circularized half-light radius of King profile, in parsecs.

We modeled the LRIS-blue spectra with the most recent version of the `alf` code (Conroy & van Dokkum 2012; Conroy et al. 2018). To improve the constraints on the stellar population parameters we stacked the 11 GC spectra, weighting by the S/N ratio. The stacked spectrum is shown in Fig. 5. The S/N ratio ranges from  $\approx 12 \text{ pix}^{-1}$  at  $\lambda = 3800 \text{ \AA}$  to  $\approx 55 \text{ pix}^{-1}$  at  $\lambda = 5400 \text{ \AA}$  (with  $1.5 \text{ \AA pix}^{-1}$ ). The best fitting model, shown in red, has  $[\text{Fe}/\text{H}] = -1.35 \pm 0.12$ ,  $[\text{Mg}/\text{Fe}] = 0.16 \pm 0.17$ , and age =  $9.3_{-1.2}^{+1.3}$  Gyr. The mass-to-light ratio is  $M/L_V = 1.8 \pm 0.2$ . The errors were determined using an MCMC fitting technique, as described in Conroy & van Dokkum (2012).

We conclude that the objects are old and metal poor. This likely applies to the entire system: the scatter in the  $V_{606} - I_{814}$  colors of the GCs is very small, and their average color is consistent with that of the diffuse galaxy light:  $\langle V_{606} - I_{814} \rangle_{\text{gc}} = 0.36 \pm 0.02$  and  $(V_{606} - I_{814})_{\text{gal}} = 0.37 \pm 0.05$ .

The  $\alpha$ -enhancement appears to be low, but typical values for globular clusters (0.3–0.5) are only  $1 - 2\sigma$  removed from the best fit. Importantly, the age (and also the  $M/L$  ratio) should be regarded as lower limits, due to the possible effects of blue horizontal branch (BHB) stars. As discussed in, e.g., Schiavon (2007) and Conroy et al. (2018) the presence of BHB stars reduces the ages that are derived from integrated-light spectra. The average spectrum of the 11 NGC1052–DF2 GCs is similar to the integrated-light spectra of Galactic GCs with  $[\text{Fe}/\text{H}] \sim -1.4$  and ages of  $\sim 12$  Gyr (see Marín-Franch et al. 2009).

## 6. DISCUSSION

We analyzed the population of globular clusters associated with the UDG NGC1052–DF2. Superficially the galaxy resembles many other UDGs. For example, the morphology of the diffuse light and the fraction of the light that is in GCs are similar to the well-studied UDG Dragonfly 17 in the Coma cluster (van Dokkum et al. 2015; Peng & Lim 2016; Beasley & Trujillo 2016). The stellar populations are also similar; the  $V_{606} - I_{814}$  colors are identical within the errors to those of Dragonfly 44 (van Dokkum et al. 2017), and Gu et al. (2017) report ages and metallicities for three Coma UDGs that are consistent with what we find here. A generic explanation for such diffuse, globular cluster-rich systems may be that they are “failed” galaxies, in which star formation terminated shortly after the metal-poor GCs appeared and before a metal-rich component began to form. This naturally explains their specific frequencies and uniform stellar populations, and is qualitatively consistent with the observation that  $S_N$  in dwarf galaxies is much higher when only metal-poor stars are considered (e.g., Larsen et al. 2014).

NGC1052–DF2 is also very *different* from other UDGs (and indeed all other known galaxies), in two distinct ways that may be related to one another. First, the luminosity function of the GCs has a narrow peak at  $M_{V,606} \approx -9.1$  (Fig. 3). This is remarkable as the canonical value of  $M_V \approx -7.5$  was thought to be universal, with only  $\sim 0.2$  mag variation between galaxies (see Rejkuba 2012). The origin of this unusual luminosity function is unknown; it could be related to enhanced hierarchi-

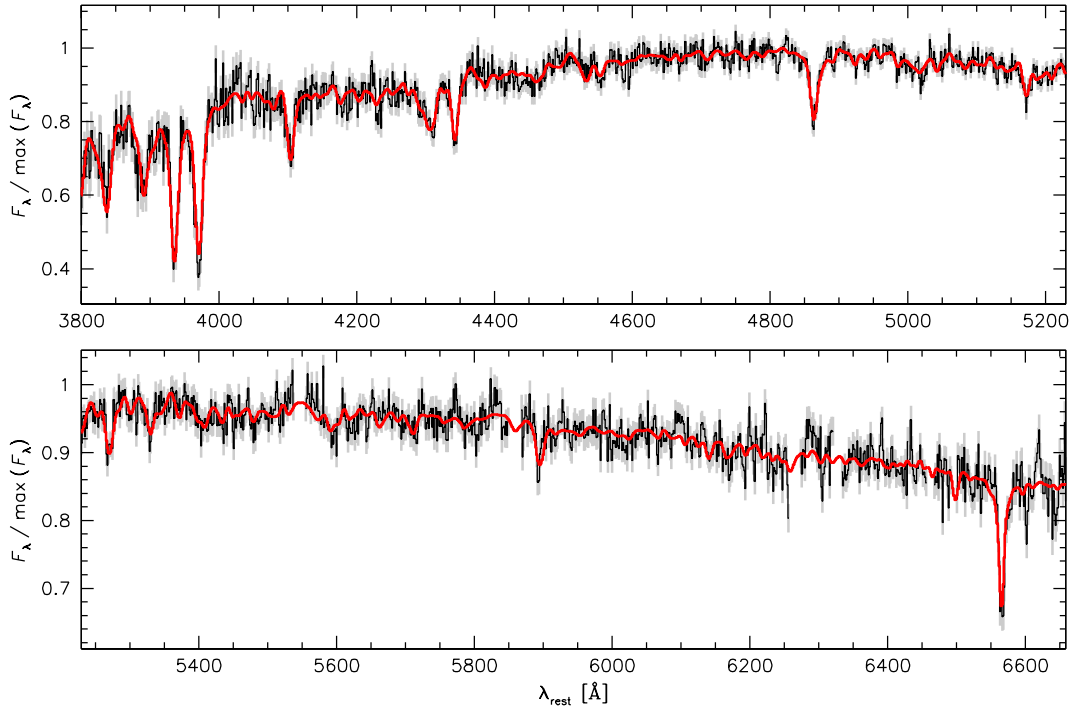


**Figure 5.** Combined Keck/LRIS spectrum of the 11 GCs, weighted by the S/N ratio. Errors are shown in grey. The best-fitting stellar population synthesis model is shown in red. This model has an age of  $9.3_{-1.2}^{+1.3}$  Gyr,  $[\text{Fe}/\text{H}] = -1.35 \pm 0.12$ , and  $[\text{Mg}/\text{Fe}] = 0.16 \pm 0.17$ . The age is a lower limit, as it does not take the possible presence of blue horizontal branch stars into account.

cal merging of lower mass clusters (S. Trujillo-Gomez et al., in prep.). The sizes and ellipticities of the GCs are different too, but this may not be very fundamental. Since  $\rho \propto M r_h^{-3}$  the GCs are a factor of  $\sim 2$  less dense than is typical. However, their virial velocities are a factor of  $\sqrt{2}$  higher, which means that their kinetic energy densities  $e_{\text{kin}} \sim P \propto \rho v^2$  are similar. Therefore, the same gas pressures were needed to form these clusters as those that led to the formation of typical Galactic GCs (see Elmegreen & Efremov 1997). The higher ellipticities may simply reflect the initial angular momentum of the GCs; as  $t_r \propto \sqrt{M} r_h^{1.5}$  the relaxation times are a factor of  $\sim 5$  longer than in typical Milky Way GCs. We note that the effects of the external gravitational potential on the structure of the GCs are likely weak, due to the lack of dark matter in NGC1052–DF2 and the high masses of the clusters (see, e.g., Goodwin 1997; Miholics et al. 2016).

The second difference is that the galaxy has no (or very little) dark matter (see vD18). This stands in stark contrast to cluster UDGs (see Beasley et al. 2016; van Dokkum et al. 2016; Mowla et al. 2017), and is inconsistent with the idea that the old, metal-poor globular cluster systems of galaxies are always closely connected to their dark matter halos. Specifically, previous studies found that the ratio between the total mass in GCs and the total (dark + baryonic) mass of galaxies is remarkably constant, with  $M_{\text{gc}}^{\text{tot}} \approx 3 \times 10^{-5} M_{\text{gal}}^{\text{tot}}$  (Blakeslee et al. 1997; Harris et al. 2015; Forbes et al. 2016). Taking  $M/L_V \approx 2$  (§5) we find  $\approx 9 \times 10^6 M_{\odot}$  for the total mass of the globular clusters in NGC1052–DF2, and in vD18 we derived a 90% upper limit of  $< 3.4 \times 10^8 M_{\odot}$  for its to-

tal galaxy mass. Therefore, the mass in the GC system is  $\gtrsim 3\%$  of the mass of the galaxy, a factor of  $\sim 1000$  higher than the Harris et al. value. The existence of NGC1052–DF2 suggests that the approximately linear correlation between GC system mass and total galaxy mass is not the result of a fundamental relation between the formation of metal-poor globular clusters and the properties of dark matter halos (as had been suggested by, e.g., Spitler & Forbes 2009; Trenti, Padoan, & Jimenez 2015; Boylan-Kolchin 2017). Instead, the correlation may be a by-product of other relations, with globular cluster formation ultimately a baryon-driven process (see, e.g., Kruijssen 2015; Mandelker et al. 2017).

Taking these ideas one step further, perhaps a key aspect of forming a UDG – or at least UDGs with many GCs – is, paradoxically, the presence of very dense gas at high redshift. After a short period of very intense star formation the gas was blown out, possibly by supernova (or black hole) feedback from the forming clumps themselves (e.g., Calura et al. 2015). If the gas contained most of the mass in the central regions of the forming galaxy this event may have led to the extreme puffing up of the inner few kpc (see also Di Cintio et al. 2017; Chan et al. 2017). The gas never returned, either because the galaxy ended up in a cluster (Dragonfly 17) or because it had very low mass (NGC1052–DF2). In this context having a massive dark matter halo is not a central aspect of UDGs, but one of several ways to reach sufficiently high gas densities for efficient globular cluster formation at early times.

Of course, all this is speculation; also, this description of events does not address the origin of  $\sim 10^{8-9} M_{\odot}$  of extremely dense gas without a dark matter halo. In this

context, an important unanswered question is whether NGC1052–DF2 is a “pathological” galaxy that is the result of a rare set of circumstances or representative of a class of similar objects. There are several galaxies in our Cycle 23 *HST* program that superficially resemble it, although none has quite as many luminous star clusters. NGC1052–DF2-like objects may have been more common in the past, as large galaxies without dark matter lead a tenuous existence; in clusters and massive groups they are easily destroyed, donating their star clusters to the intracluster population of GCs and ultra compact dwarfs (UCDs). We note that progenitors of galaxies like NGC1052–DF2 could readily be identified in JWST observations if its luminous GCs did indeed form within  $\sim 10^8$  yr of each other in a dense region.

Finally, we briefly discuss whether the compact objects in NGC1052–DF2 should be considered globular clusters at all. In terms of their average luminosity and size they are intermediate between GCs and UCDs (see, e.g., Brodie et al. 2011), and this question hinges on whether we focus on the population or on individual objects: the population characteristics are unprecedented,

but for each individual object in NGC1052–DF2 a match can be found among the thousands of GCs with measured sizes and luminosities in other galaxies (e.g., Larsen et al. 2001; Barmby et al. 2007). Intriguingly, in terms of their sizes, flattening, stellar populations, and luminosities the 11 compact star clusters are remarkably similar to  $\omega$  Centauri – an object whose nature has been the topic of decades of debate (see, e.g., Norris & Da Costa 1995).

Support from *HST* grant HST-GO-14644 and NSF grants AST-1312376, AST-1515084, AST-1518294, and AST-1613582 is gratefully acknowledged. JMDK gratefully acknowledges funding from the German Research Foundation (DFG) in the form of an Emmy Noether Research Group (grant number KR4801/1-1) and from the European Research Council (ERC) under the European Union’s Horizon 2020 research and innovation programme via the ERC Starting Grant MUSTANG (grant agreement number 714907). AJR is a Research Corporation for Science Advancement Cottrell Scholar.

## REFERENCES

- Abraham, R. G. & van Dokkum, P. G. 2014, *PASP*, 126, 55  
 Amorisco, N. C., Monachesi, A., & White, S. D. M. 2018, *MNRAS*, 475, 4235  
 Barmby, P., McLaughlin, D. E., Harris, W. E., Harris, G. L. H., & Forbes, D. A. 2007, *AJ*, 133, 2764  
 Beasley, M. A., Romanowsky, A. J., Pota, V., Navarro, I. M., Martínez Delgado, D., Neyer, F., & Deich, A. L. 2016, *ApJL*, 819, L20  
 Beasley, M. A. & Trujillo, I. 2016, *ApJ*, 830, 23  
 Beers, T. C., Flynn, K., & Gebhardt, K. 1990, *AJ*, 100, 32  
 Behroozi, P. S., Marchesini, D., Wechsler, R. H., Muzzin, A., Papovich, C., & Stefanon, M. 2013, *ApJL*, 777, L10  
 Bertin, E. & Arnouts, S. 1996, *A&AS*, 117, 393  
 Blakeslee, J. P., Cantiello, M., Mei, S., Côté, P., Barber DeGraaff, R., Ferrarese, L., Jordán, A., Peng, E. W., et al. 2010, *ApJ*, 724, 657  
 Blakeslee, J. P., Tonry, J. L., & Metzger, M. R. 1997, *AJ*, 114, 482  
 Bohlin, R. C. 2016, *AJ*, 152, 60  
 Boylan-Kolchin, M. 2017, *MNRAS*, 472, 3120  
 Brodie, J. P., Romanowsky, A. J., Strader, J., & Forbes, D. A. 2011, *AJ*, 142, 199  
 Calura, F., Few, C. G., Romano, D., & D’Ercole, A. 2015, *ApJL*, 814, L14  
 Chan, T. K., Kereš, D., Wetzel, A., Hopkins, P. F., Faucher-Giguère, C.-A., El-Badry, K., Garrison-Kimmel, S., & Boylan-Kolchin, M. 2018, *MNRAS*, submitted (arXiv:1711.04788)  
 Conroy, C. & van Dokkum, P. 2012, *ApJ*, 747, 69  
 Conroy, C., Villaume, A., van Dokkum, P. G., & Lind, K. 2018, *ApJ*, 854, 139  
 Di Cintio, A., Brook, C. B., Dutton, A. A., Macciò, A. V., Obreja, A., & Dekel, A. 2017, *MNRAS*, 466, L1  
 Elmegreen, B. G. & Efremov, Y. N. 1997, *ApJ*, 480, 235  
 Forbes, D. A., Alabi, A., Romanowsky, A. J., Brodie, J. P., Strader, J., Usher, C., & Pota, V. 2016, *MNRAS*, 458, L44  
 Goodwin, S. P. 1997, *MNRAS*, 286, L39  
 Gu, M., Conroy, C., Law, D., van Dokkum, P., Yan, R., Wake, D., Bundy, K., Merritt, A., et al. 2018, *ApJ*, submitted (arXiv:1709.07003)  
 Harris, W. E. 1996, *AJ*, 112, 1487  
 Harris, W. E., Harris, G. L., & Hudson, M. J. 2015, *ApJ*, 806, 36  
 King, I. 1962, *AJ*, 67, 471  
 Koekemoer, A. M., Faber, S. M., Ferguson, H. C., Grogin, N. A., Kocevski, D. D., Koo, D. C., Lai, K., Lotz, J. M., et al. 2011, *ApJS*, 197, 36  
 Kruijssen, J. M. D. 2015, *MNRAS*, 454, 1658  
 Larsen, S. S., Brodie, J. P., Forbes, D. A., & Strader, J. 2014, *A&A*, 565, A98  
 Larsen, S. S., Brodie, J. P., Huchra, J. P., Forbes, D. A., & Grillmair, C. J. 2001, *AJ*, 121, 2974  
 Mandelker, N., van Dokkum, P. G., Brodie, J. P., van den Bosch, F. C., & Ceverino, D. 2018, *ApJ*, in press (arXiv:1711.09108)  
 Marín-Franch, A., Aparicio, A., Piotto, G., Rosenberg, A., Chaboyer, B., Sarajedini, A., Siegel, M., Anderson, J., et al. 2009, *ApJ*, 694, 1498  
 Merritt, A., van Dokkum, P., Abraham, R., & Zhang, J. 2016, *ApJ*, 830, 62  
 Miholics, M., Webb, J. J., & Sills, A. 2016, *MNRAS*, 456, 240  
 Moster, B. P., Naab, T., & White, S. D. M. 2013, *MNRAS*, 428, 3121  
 Mowla, L., van Dokkum, P., Merritt, A., Abraham, R., Yagi, M., & Koda, J. 2017, *ApJ*, 851, 27  
 Norris, J. E. & Da Costa, G. S. 1995, *ApJ*, 447, 680  
 Oke, J. B., Cohen, J. G., Carr, M., Cromer, J., Dingizian, A., Harris, F. H., Labrecque, S., Lucinio, R., et al. 1995, *PASP*, 107, 375  
 Peng, C. Y., Ho, L. C., Impey, C. D., & Rix, H.-W. 2002, *AJ*, 124, 266  
 Peng, E. W. & Lim, S. 2016, *ApJL*, 822, L31  
 Rejkuba, M. 2012, *Ap&SS*, 341, 195  
 Schiavon, R. P. 2007, *ApJS*, 171, 146  
 Schlafley, E. F., & Finkbeiner, D. P. 2011, *ApJ*, 737, 103  
 Sersic, J. L. 1968, *Atlas de galaxias australes* (Cordoba, Argentina: Observatorio Astronomico, 1968)  
 Skelton, R. E., Whitaker, K. E., Momcheva, I. G., Brammer, G. B., van Dokkum, P. G., Labbé, I., Franx, M., van der Wel, A., et al. 2014, *ApJS*, 214, 24  
 Spitler, L. R. & Forbes, D. A. 2009, *MNRAS*, 392, L1  
 Trenti, M., Padoan, P., & Jimenez, R. 2015, *ApJL*, 808, L35  
 van Dokkum, P., Abraham, R., Brodie, J., Conroy, C., Danieli, S., Merritt, A., Mowla, L., Romanowsky, A., et al. 2016, *ApJL*, 828, L6  
 van Dokkum, P., Abraham, R., Romanowsky, A. J., Brodie, J., Conroy, C., Danieli, S., Lokhorst, D., Merritt, A., et al. 2017, *ApJL*, 844, L11  
 van Dokkum, P., Danieli, S., Cohen, Y., Merritt, A., Romanowsky, A. J., Abraham, R., Brodie, J., Conroy, C., et al. 2018, *Nature*, in press  
 van Dokkum, P. G., Abraham, R., Merritt, A., Zhang, J., Geha, M., & Conroy, C. 2015, *ApJL*, 798, L45